A framework for chaotic signature classification: Insights from Chua’s circuit

Impact of Electromagnetic Interference From Consumer Electronics and Bluetooth Crowding on GNSS-Based Performance in Mobile Devices

Luca Morichi, *Student Member, IEEE*, Iman Ebrahimi Mehr, Mikhael Russo, Cristian Carallo, Riccardo Tommasi, and Andrea Nardin, *Member, IEEE*

***Abstract*—This article explores the impact of electromagnetic interference from consumer electronics and common household appliance on the performance of Global Navigation Satellite System (GNSS) receivers in smartphones. As GNSS signals are weak and susceptible to external noise and interference, consumer appliances can introduce spurious emissions within GNSS frequency bands, leading to signal degradation. To investigate this, we conducted a series of controlled experiments simulating typical smartphone usage in proximity to different sources of EMI among household appliances (i.e., a microwave oven) and consumer electronics (i.e., Wi-Fi and Bluetooth devices), ultimately focusing on a dense Bluetooth environment. Our analysis reveals that the microwave oven can induce severe GNSS signal degradation, with substantial automatic gain control and C/N_0 drops (up to 2.3 dB-Hz) and significant satellite availability loss (up to 18%), particularly in close-range configurations, leading to positioning root-mean-square error (RMSE) increases exceeding 7 m. In addition, Wi-Fi interference resulted in moderate reductions in signal quality, with positioning RMSE increases of less than 2 m in most scenarios. In contrast, Bluetooth exhibited negligible effects under tested conditions. These findings suggest potential implications for indoor navigation applications and underscore the importance of further improvements in interference mitigation for consumer GNSS devices.**

***Index Terms*—Android, Bluetooth, consumer electronics, consumer technology, electromagnetic interference (EMI), Global Navigation Satellite System (GNSS), household appliances, satellite navigation, smartphone, Wi-Fi.**

I. Introduction

GLOBAL Navigation Satellite System (GNSS) receivers embedded in smartphones play a pivotal role in navigation, location-based services, and time synchronization [1]. Their widespread adoption has made ubiquitous positioning a key enabler for applications ranging from turn-by-turn navigation to emergency response [2] and autonomous systems [3]. However, despite significant advances in the design of GNSS receivers [4], GNSS chipsets remains highly susceptible to electromagnetic interference (EMI), particularly in indoor and semi-indoor environments. Since smartphone GNSS receivers operate with signals received at extremely low power levels—typically around −130 dBm or lower at Earth's surface [5]—external noise and interference sources can significantly degrade their performance [6].

The consequences of EMI on GNSS receivers can range from minor disturbances to complete signal loss. In severe cases, the interference can lead to the loss of satellite signals, causing navigation and timing outages. Even brief periods of interference may result in position, velocity, and time (PVT) errors, with position jumps or inaccurate velocity readings being particularly problematic in dynamic environments.

Previous studies have extensively examined intentional interference sources, such as jammers and spoofers [7], [8], also from a smartphone perspective [9], [10], [11], [12]. Intentional and unintentional EMI affecting GNSS bands has also been investigated through large-scale spectrum monitoring and measurement initiatives, including the STRIKE3 project [13], which focuses on the detection, classification, and characterization of radio frequency (RF) interference in GNSS bands. However, the receiver-level impact of unintentional EMI generated by common household appliances and consumer electronics on commercial smartphone GNSS receivers, particularly in close-proximity and dense RF usage scenarios, and quantified in terms of front-end response, signal quality, and PVT performance, remains unexplored [14], [15]. Many of these potential EMI sources are ubiquitous in residential, commercial, and industrial settings, yet their potential to interfere with GNSS signals in smartphones has received limited attention. Given the increasing reliance on GNSS-based services indoors and in transition zones (e.g., building entrances), understanding the impact of these interference sources is crucial for improving GNSS receiver resilience.

Although GNSS usage is limited indoors, many emerging applications leverage hybrid positioning systems (e.g., combining GNSS with Wi-Fi, Bluetooth, or inertial sensors) and improved receiver technologies to support location-based services in large

Received 17 November 2025; revised 12 February 2026 and 9 April 2026; accepted 10 April 2026. Date of publication 16 April 2026; date of current version 27 April 2026. *(Corresponding author: Andrea Nardin.)*

Luca Morichi and Andrea Nardin are with the Department of Electronics and Telecommunications (DET), Politecnico di Torino, Turin 10129, Italy (e-mail: luca.morichi@polito.it; andrea.nardin@polito.it).

Iman Ebrahimi Mehr is with the LINKS Foundation, AI, Data and Space (ADS) domain, Turin, Italy (e-mail: iman.ebrahimi@linksfoundation.com).

Mikhael Russo, Cristian Carallo, and Riccardo Tommasi are with the Politecnico di Torino, Turin 10129, Italy (e-mail: s329165@studenti.polito.it; s322458@studenti.polito.it; s323816@studenti.polito.it).

Digital Object Identifier 10.1109/JISPIN.2026.3684360

indoor areas, such as malls, airports, or warehouses [16], [17], [18], [19], [20]. In these cases, even weak GNSS signals can contribute to the overall positioning solution. Unintentional EMI in these contexts could degrade the performance of GNSS-based services, causing intermittent errors in location tracking, particularly in moments where GNSS still has a role in the PVT estimation process.

Microwave ovens are one of the most powerful household sources of RF radiation, operating at 2.45 GHz within the industrial, scientific, and medical (ISM) band [21]. While this frequency does not directly overlap with GNSS bands, such as L1 (1.57542 GHz) or L2 (1.2276 GHz) [22], microwave ovens are not perfectly shielded, leading to leakage of spurious emissions that can extend into adjacent frequencies. The potential for interference is exacerbated by the significant disparity in signal power between GNSS signals and microwave oven emissions, which operate in the range of hundreds of watts [5]. This leakage can introduce RF noise and distortions in nearby GNSS receivers, leading to signal tracking errors. The effects of microwave interference are particularly concerning for Doppler measurements, which rely on precise frequency tracking to estimate velocity.

Wi-Fi routers and Bluetooth devices also operate within the 2.4 GHz ISM band, overlapping with microwave oven emissions and producing RF interference in crowded environments [23], [24]. Smartphones are frequently used near high-density wireless networks, where multiple Wi-Fi access points and Bluetooth accessories compete for spectrum. This creates a scenario where cochannel interference, intermodulation distortions, and spurious emissions can contribute to GNSS signal degradation [25], [26]. As a result, Wi-Fi routers can generate harmonic emissions that extend beyond 2.4 GHz, potentially affecting GNSS bands, particularly in environments with multiple active devices. Moreover, Bluetooth gimbals and earphones continuously transmit data in short bursts, which may introduce localized interference patterns affecting GNSS tracking. Nonetheless, such devices are fairly common also in outdoor environments. Given the increasing integration of smartphones with dense Internet of Things (IoT) ecosystems, these interference sources must be accounted for when assessing GNSS performance in real-world conditions.

To systematically evaluate the impact of consumer electronics on smartphone GNSS receivers, this study, which is an extension of a proceedings paper, conducted a series of controlled experiments replicating real-world usage scenarios and analyzing the impact of a microwave oven, a Wi-Fi router, and Bluetooth accessories. Although Bluetooth devices operate at relatively low transmit power, their increasing ubiquity in modern environments—often with several accessories active simultaneously—raises the potential for aggregate interference effects. To examine this, a crowded Bluetooth environment was also tested in this extended work to challenge GNSS reception and emulate realistic dense wireless conditions that may arise during everyday smartphone use. The goal is to measure the impact at three distinct levels: 1) the signal level; 2) the measurement level; and 3) the state estimation level. The adopted figure of merits (FoMs)—necessarily limited by the accessibility to intermediate observables on smartphones [27], [28]—are therefore designed to provide a comprehensive understanding of how interference affects the receiver's performance, from the impact on the automatic gain control (AGC), to the measured carrier-to-noise-density ratio (C/N_0), and PVT solution. In addition, the metrics are aggregated using averages and root-mean-square errors (RMSEs) to facilitate comparison across different experiments, interference sources, and device configurations. Fig. 1 provides a high-level description of the GNSS receiver processing stages, with the monitoring taps highlighted. The interested reader is referred to [29] for a more detailed description of the receiver architecture and associated monitoring points and to [27], [28], and [30] for an overview on GNSS observables available in smart devices.

The results provide insights into the relative severity of interference across different consumer electronics and wireless devices, highlighting which devices pose the greatest risk to GNSS accuracy in smartphones. By characterizing these effects, this study contributes to the broader goal of improving interference mitigation techniques in smartphone GNSS receivers.

This article extends and significantly expands a preliminary study previously presented in [31]. The original contribution introduced an experimental assessment of EMI from common consumer electronics on smartphone GNSS performance using raw measurements. The present journal version includes several major technical extensions. First, the computation of the adopted FoMs has been refined by focusing exclusively on GNSS-based PVT solutions derived from Android raw measurements, rather than on fused location solutions, leading to updated quantitative results throughout this article. Second, a new performance metric—the velocity RMSE—has been introduced to evaluate the impact of EMI on Doppler-based velocity estimation, and all experimental analyses have been extended accordingly. Third, a new experimental scenario addressing EMI in a crowded Bluetooth environment has been designed and analyzed, providing a more challenging and realistic representation of modern wireless conditions and extending the previous single-device Bluetooth interference experiments.

In light of the above, this work presents a systematic experimental assessment of unintentional EMI from common consumer electronics—including microwave ovens, Wi-Fi routers, and Bluetooth devices—on GNSS performance in smartphones, addressing what is, to the best of the authors' knowledge, an unexplored problem in the literature. The analysis is conducted across multiple stages of the receiver processing chain, enabling a comprehensive characterization of interference effects. The experimental campaign is designed to replicate realistic usage conditions through controlled yet representative scenarios, including close-proximity configurations and dense wireless environments.

The rest of this article is organized as follows. Section II describes the experimental methodology and the FoMs adopted. Section III presents the results from the testing campaigns. Finally, Section IV concludes this article.

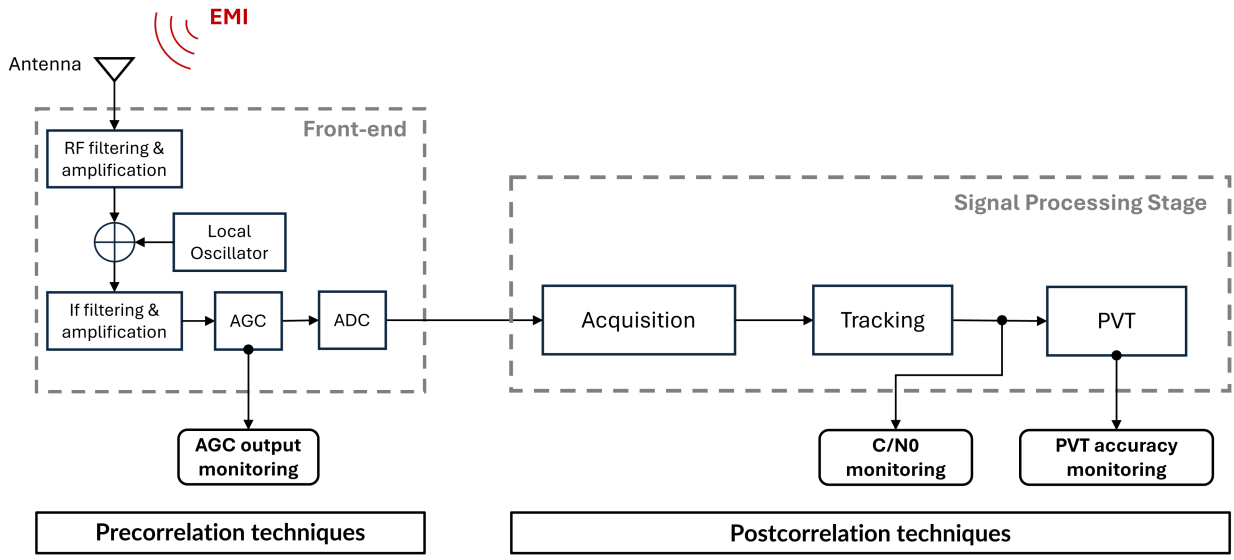

Fig. 1. High-level block diagram of a GNSS receiver highlighting the three monitoring points used for the analysis: AGC, C/N_0, and PVT. Figure adapted from [29].

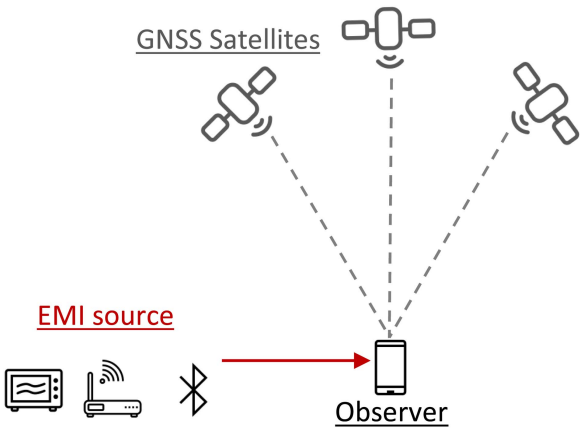

Fig. 2. Pictorial representation of the experimental setup, showing GNSS satellites, EMI sources (microwave, Wi-Fi, and Bluetooth), and the smartphone receiver.

II. Methodology

This study involved controlled experiments designed to simulate typical smartphone usage in three different scenarios. The first scenario considers proximity to a microwave oven. The second scenario involves the use of a wireless router, differentiating between urban environment and low-elevation blockage. Finally, the third scenario examines interference from Bluetooth devices, first, by specifically focusing on headphones and a gimbal, and second, addressing a crowded Bluetooth environment. A pictorial representation of the test environment is reported in Fig. 2.

All tested devices, since sold in Europe are CE-certified. As such, they comply with the applicable electromagnetic compatibility requirements under Directive 2014/30/EU [32]. These devices also conform to the following relevant technical standards: ETSI EN 300 328, ETSI EN 301 908 series, and ETSI EN 55011 / CISPR 11. The above standards define limits on transmitted power, out-of-band emissions, and spurious radiated emissions, typically expressed relative to the carrier power and evaluated over standardized measurement bandwidths. While compliance with these spectral masks ensures that devices do not cause harmful interference to typical radio services, it does not preclude the presence of low-level broadband noise, harmonics, or spurious components [33]. Due to the extremely low received power of GNSS signals, such emissions—although compliant with regulatory limits—may still result in measurable performance degradation when consumer devices operate in close proximity to GNSS receivers, particularly in near-field conditions.

Experiments were conducted outdoor using different smartphone models (Oppo Reno 11F 5 G (CPH2603), Oneplus 8 IN2013, Motorola Razr 40, and OnePlus Nord 40) to examine the impact of EMI on the smartphones' GNSS chipset. The analysis was necessarily limited to Android devices (no iOS), as access to raw GNSS measurements is currently restricted to this platform. This also constrained the depth of the investigation into the underlying interference mechanisms due to the limited transparency of the algorithms used to compute some of the exposed metrics [9]. Nevertheless, we deliberately selected smartphones featuring different GNSS chipsets to introduce hardware diversity. For this initial exploratory study, the number of available devices was limited.

The phones were not connected to the Internet during the whole duration of the experiments to favor the genuineness of raw GNSS measurements, limiting external aiding or corrections. Given that the smartphones had been powered on for several hours prior to the measurements, the GNSS receivers are considered to be operating under a hot start condition [1, pp. 33–34].

Notably, in each scenario, the duration of the EMI phase was strictly set to 3 min for all cases, except for the Wi-Fi case, where

TABLE I
EXPERIMENTAL SCENARIO COMMON SETTINGS

Parameter	*Value*
Experiment Duration	10 min
Data collection start time	t_0
Interference Duration	3 (from $t_0 + 5$ to $t_0 + 8$) min[a]
Location	45.0627°N, 7.6622°E
Receiver's dynamic conditions	Static

[a] Exception made for the Wi-Fi case: 4 (from $t_0 + 4$ to $t_0 + 8$) min.

it was extended to 4 min to facilitate setup and account for the modem power-up transient. This ensured a comparable common ground without distinctions. For the sake of completeness, all parameters shared across the various experiments and scenarios are presented in Table I.

Data were collected using the GNSS Logger app [34], developed by Google, which records measurements from the smartphone's internal GNSS receiver in a textual log format. The dataset includes, among others, AGC, C/N_0, satellite visibility per constellation, and receiver position estimates (provided in GNSS-only, fused, and network-aided modes), although only GNSS-based solutions are considered in this work.

It is important to acknowledge several constraints associated with the adopted experimental methodology, which relies on the use of commercial off-the-shelf (COTS) devices, which is inherent to the objective of assessing interference effects under realistic conditions involving consumer electronics and commercial smartphones. On the receiver side, the use of commercial smartphones limits access to low-level receiver information and internal processing details, thereby reducing the ability to fully interpret certain observables and to isolate specific interference mechanisms. On the interference side, the emission characteristics of consumer-grade devices are not fully known nor directly controllable, which constrains the repeatability of the experiments and prevents a detailed spectral characterization of the interference.

In this context, it is worth highlighting that the AGC metric available on Android devices presents several limitations and inconsistencies that must be considered when interpreting the results. Specifically, the response of AGC to EMI can vary across devices, with some showing an increase and others a decrease under similar conditions. Moreover, AGC values are typically reported on a relative scale and may undergo periodic rescaling, potentially obscuring long-term trends. An additional limitation is that AGC measurements are only available when GNSS signals are being tracked, preventing their use in distinguishing between interference and signal attenuation in the absence of logged GNSS data. These factors affect the reliability of AGC for certain applications, such as interference detection. For a more detailed discussion, refer to [9] and [35]. Furthermore, other receiver-related parameters, such as antenna characteristics and phase center information, are generally not accessible or not fully specified in commercial smartphones, further limiting the interpretability of GNSS observables [36], [37]. These aspects should be taken into account when interpreting and generalizing the presented results.

A. Figures of Merit

With reference to Fig. 1, which illustrates the GNSS receiver processing chain and the associated monitoring taps, the following FoMs are used to quantify the impact of EMI by comparing measurements collected before the interference with those acquired during the EMI event (denoted by the diacritical mark $\sim$). Data recorded after the interference are not considered, in order to avoid postinterference transient effects. All metrics are defined such that larger positive values indicate a stronger detrimental impact of EMI.

1) *Average drop of the AGC:* It is determined by computing the mean AGC before (α) and during interference ($\tilde{\alpha}$) for each constellation i and then averaging the results across all of them, yielding

$$\Delta\text{AGC} = \frac{1}{M}\sum_{i=1}^{M}(\alpha_i - \tilde{\alpha}_i).$$

2) *Average drop of the C/N_0:* It is calculated by comparing the mean C/N_0 over time before (γ) and during the interference phase ($\tilde{\gamma}$) for each satellite, followed by an average across all the persistently observed satellites ($\bar{N}$), resulting in

$$\Delta\text{C/N}_0 = \frac{1}{\bar{N}}\sum_{i=1}^{\bar{N}}(\gamma_i - \tilde{\gamma}_i).$$

3) *Availability of satellites:* It is assessed by the average number of tracked satellites in both interference-free (N) and EMI conditions ($\tilde{N}$), measuring the relative decrease, and representing it as a percentage so that

$$\Delta\text{N} = \left(1 - \frac{\tilde{N}}{N}\right)\cdot 100\%.$$

In addition, the RMSE is used as a statistical indicator of the average magnitude of the positioning and velocity estimation error over a given observation window. In this work, the reference solution is defined as the median estimate computed over the considered time interval. The RMSE is then computed as

$$\text{RMSE} = \sqrt{\frac{1}{T}\sum_{t=1}^{T}\|\mathbf{x}(t) - \hat{\mathbf{x}}\|^2} \tag{1}$$

where $\mathbf{x}(t)$ denotes the estimated state vector at time t, including either position or velocity components depending on the considered metric, and $\hat{\mathbf{x}}$ is the corresponding median value, computed from the position estimate time series prior to the interference event. The RMSE-based metrics considered in this work are as follows.

1) *Position RMSE drop:* It is computed from the RMSE of the 3-D position error before (ϵ) and during interference ($\tilde{\epsilon}$), where both are defined using (1), leading to

$$\Delta\text{RMSE}_p = \tilde{\epsilon} - \epsilon.$$

2) *Velocity RMSE drop:* It is computed analogously from the velocity RMSE before (η) and during interference

($\tilde{\eta}$), both defined using (1), yielding

$$\Delta\text{RMSE}_v = \tilde{\eta} - \eta.$$

Python scripts were employed to derive the FoMs discussed here, specifically to aggregate all results and present them in a compact form using heatmaps, as shown in Section III.

B. Household Appliance Interference

The experiment was conducted in an open courtyard of a residential building in downtown Turin, characterized by the presence of surrounding buildings on all four sides while maintaining an unobstructed line of sight to the sky. A foldable table was positioned at the center of the courtyard, and a microwave oven was placed on top to investigate the effects of microwave interference on GNSS signal reception (see Fig. 3).

Three experimental configurations were employed, with the relative positioning of the mobile devices varied while ensuring that the microwave oven remained stationary throughout the tests. The experimental configurations consisted of mobile devices positioned in direct proximity to the microwave oven: 1) against the lower front panel of the microwave door [see Fig. 3(a)]; 2) on the upper surface at its approximate center [see Fig. 3(b)]; and 3) in contact with the lower left-hand side of the appliance [see Fig. 3(c)].

Baseline GNSS measurements were recorded for 5 min before the microwave interference. Each experimental run lasted 10 min, with the microwave oven activated at the 5-min mark, operating at 900 W for 3 min. After the baseline phase, the microwave oven Whirlpool Cook30 was powered on to induce interference and disconnected at the eight-minute mark to cease operation. Throughout the experiment, the microwave oven remained closed and was unplugged except during the interference phase.

C. Wi-Fi Interference

Two experiments were conducted to analyze the impact of Wi-Fi-induced interference on GNSS performance under different environmental conditions. The two experiments aim to compare 1) urban environment with 2) low-elevation blockage scenarios. The first experiment took place in the same courtyard in central Turin described in Section II-B, while the second experiment was conducted in a below-ground courtyard of Politecnico di Torino, in Fig. 4(b).

In the first experiment, the router was placed on a foldable table at the center of a residential courtyard in downtown Turin, as in Fig. 4(a). The smartphones were positioned directly on top of the modem router (TP-Link TD-W8961 N). At the fourth-minute mark, the router was connected to a power source and at the fifth minute, the Motorola smartphone was connected to the router's network and began generating web traffic. The router was powered off at the eighth minute, after which GNSS measurements continued for the final 2 min.

The setup of the second experiment was identical to that of the first. At the fourth minute, the router was powered ON, and two iPads Air 4th Gen (Wi-Fi) connected to the network. Using a ping application [38], the iPads generated network traffic by pinging each others. The router was powered off at the eighth minute to stop the interference.

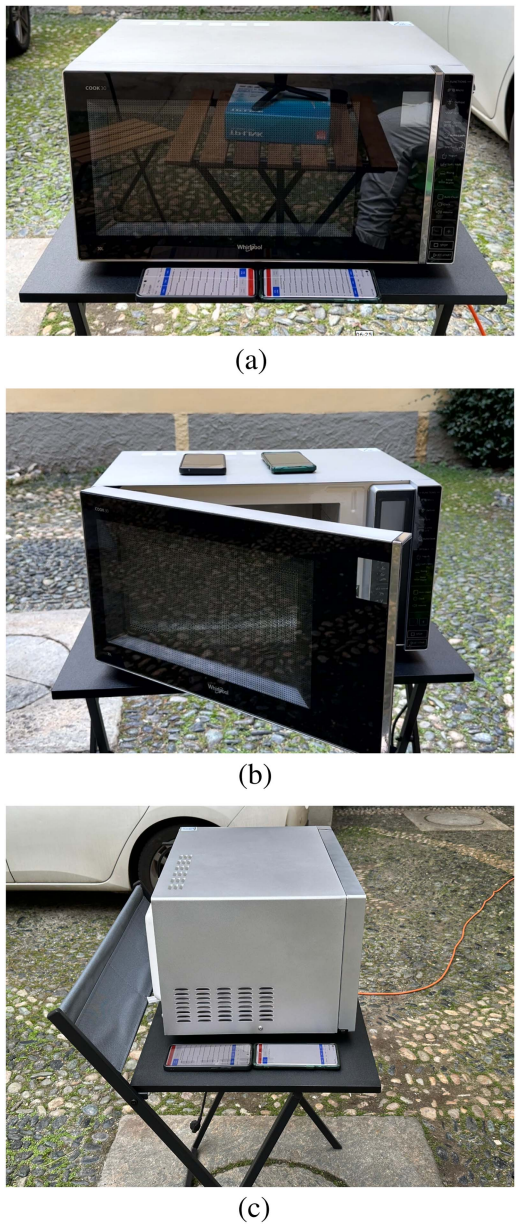

Fig. 3. Configurations for the microwave oven experiment. (a) Front setup. (b) Over setup. (c) Side setup.

D. Bluetooth Interference

1) Interference From Individual Bluetooth Devices: A first set of experiments was conducted to analyze basic Bluetooth interference in two different environments. The first experiment, performed in the below-ground courtyard of Politecnico di Torino, examined interference from a DJI Osmo Mobile 6 gimbal. The second, conducted in the residential courtyard described in Section II-B, focused on interference from Samsung Galaxy Buds 2 headphones.

In the first experiment [see Fig. 5(a)], Bluetooth interference was induced by placing a DJI Osmo Mobile 6 gimbal on a

(a)

(b)

Fig. 4. Configurations for the Wi-Fi experiment. (a) Experimental setup. (b) Campus courtyard.

(a)

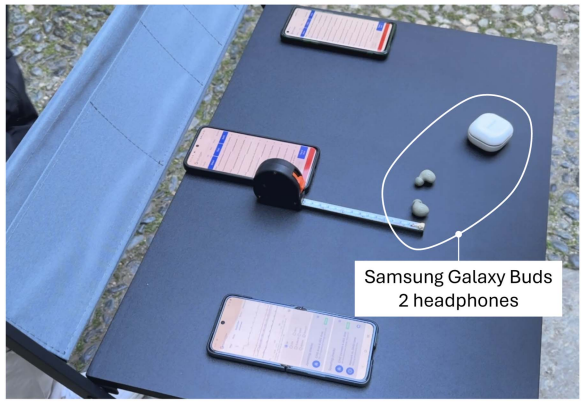

(b)

Fig. 5. Configurations for the individual Bluetooth experiment. (a) Phones and gimbal. (b) Phones and headphones.

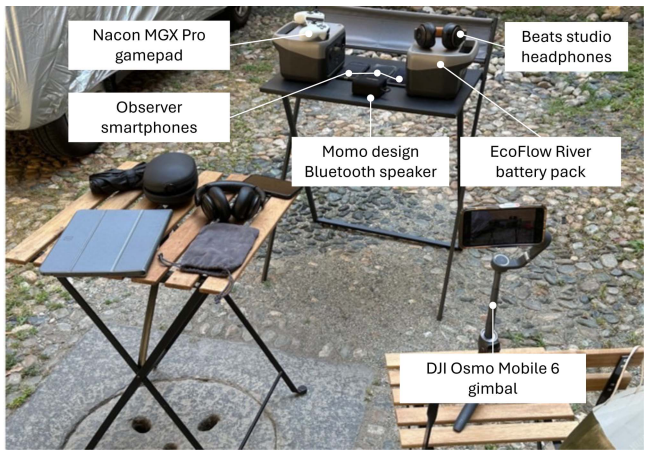

Fig. 6. Configuration for the crowded Bluetooth experiment.

cement table, with the Oppo Reno F11 5 G mounted on it and the OnePlus 8 beside it. At the 5-min mark, the Gimbal was paired with an iPhone 14 Pro Max, and moved its arm for 3 min. Then, it was then turned OFF, and the phones were monitored for the remaining 2 min.

For the second experiment, the setup is shown in Fig. 5(b). The Bluetooth headphones and phones were placed on the table, and the distance between them was varied [1) 10 cm, 2) 1 m, 3) 3 m, and 4) 15 m]. The experiment lasted for 10 min, during which, at the 5-min mark, the Samsung Galaxy Buds 2 were connected to the Oppo phone, and music started playing. The active Bluetooth transmission lasted for 3 min, after which the Bluetooth connection on the Oppo was disabled. Meanwhile, throughout the entire experiment, both the other two smartphones and the Oppo (actively involved in the Bluetooth connection) continued performing stationary measurements.

2) Interference in a Crowded Bluetooth Environment: To assess the effects of dense Bluetooth activity on GNSS reception, a dedicated experiment was conducted to emulate a crowded Bluetooth environment. Three experimental sessions, conducted in the courtyard described in Section II-B, were performed under identical spatial and device configurations, differing only in the configuration of the smartphones used as observers. Specifically, three operating conditions of the observers were tested, lasting for the whole experiment duration: 1) Flight mode ON with Bluetooth OFF; 2) Flight mode OFF with Bluetooth OFF; and 3) Flight mode OFF with Bluetooth enabled also on the observer devices.

The experiment was carried out in a fixed setup including multiple active Bluetooth links to reproduce a realistic interference scenario (see Fig. 6). In this configuration, Beats Studio headphones were paired to an iPad, a Bluetooth speaker to an iPhone 11 Pro Max, a Bluetooth joystick to an iPad (actively operated

TABLE II
DEVICES INVOLVED IN EACH EXPERIMENTAL SCENARIO

Exp. ID	Observers (Devices Under Test)	Interferers (EMI Source)	Configurations
MW-1	Oppo Reno, OnePlus 8	Microwave oven	(*i*) front, (*ii*) over, (*iii*) side
WF-1	Oppo Reno, OnePlus 8	TP-Link TD-W8961N router, Motorola Razr 40	(*i*) urban environment
WF-2	Oppo Reno, OnePlus 8	TP-Link TD-W8961N router, 2× iPad Air (4th Gen)	(*ii*) low-elevation blockage
BT-1	Oppo Reno, OnePlus 8, Motorola Razr 40	DJI Osmo Mobile 6 gimbal	(*i*) mounted, fixed distance
BT-2	Oppo Reno, OnePlus 8, Motorola Razr 40	Samsung Galaxy Buds 2 headphones	(*i*) 10 cm, (*ii*) 1 m, (*iii*) 3 m, (*iv*) 15 m
BT-3	Motorola Razr 40, OnePlus Nord 40, OnePlus 8	iPhone 7 Plus, iPhone 11 Pro Max, iPhone 14 Pro Max, iPad Pro 12.9 (3rd Gen), Beats Studio headphones, DJI Osmo Mobile 6, Nacon MGX Pro gamepad (iOS), Momo Design Bluetooth speaker, 2× EcoFlow River batteries	(*i*) Flight mode ON, Bluetooth OFF; (*ii*) Flight mode OFF, Bluetooth OFF; (*iii*) Flight mode OFF, Bluetooth ON

during the interference phase), a DJI Osmo Mobile 6 gimbal to an iPhone 7 Plus, and two portable EcoFlow River 2 battery packs to an iPhone 14 Pro Max. The observer smartphones used for GNSS data collection were a Motorola Razr 40, a OnePlus Nord 40, and a OnePlus 8. A summary of the devices involved and their experimental configurations is reported in Table II.

III. RESULTS AND DISCUSSION

This section presents and analyzes aggregated experimental results to evaluate the impact of interference in each scenario.

A. Household Appliances Interference

This section presents the experimental results for the microwave oven case. Fig. 7 presents aggregated heatmaps of all FoMs presented in Section II-A for each smartphone and setup. On the rows of each heatmap, the two smartphone models under test are reported, while the columns shows the three setup configurations, "front," "over," and "side," as depicted in Fig. 3. Each cell of the heatmaps contains two numerical values: the larger bold number represents the actual drop, whereas the smaller number below corresponds to the nominal value of the respective FoMs, i.e., the value measured before the interference source was activated.

An example of AGC and C/N_0 metrics evolutions as time-series, from which heatmaps are derived, is reported in Fig. 8 for the "side" configuration.

Notice that the GNSS receiver's analog front end collects all signals within a frequency band. A single per-band AGC loop continuously adjusts receiver gain to keep the downconverted composite signal within an optimal dynamic range, based on

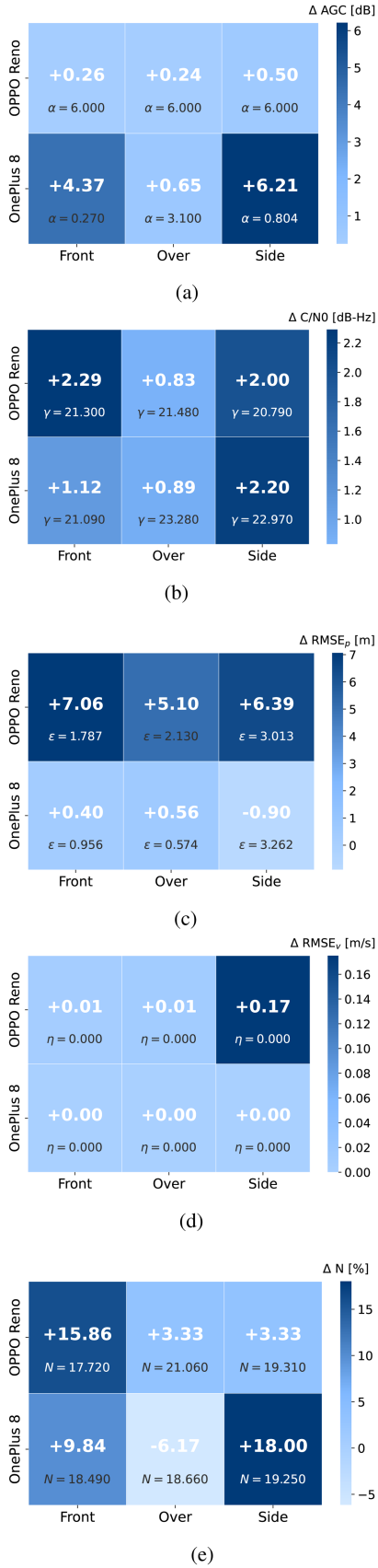

Fig. 7. FoMs for the microwave oven experiments (MW-1). (a) ΔAGC. (b) $\Delta C/N_0$. (c) ΔRMSE$_p$. (d) ΔRMSE$_v$. (e) ΔN.

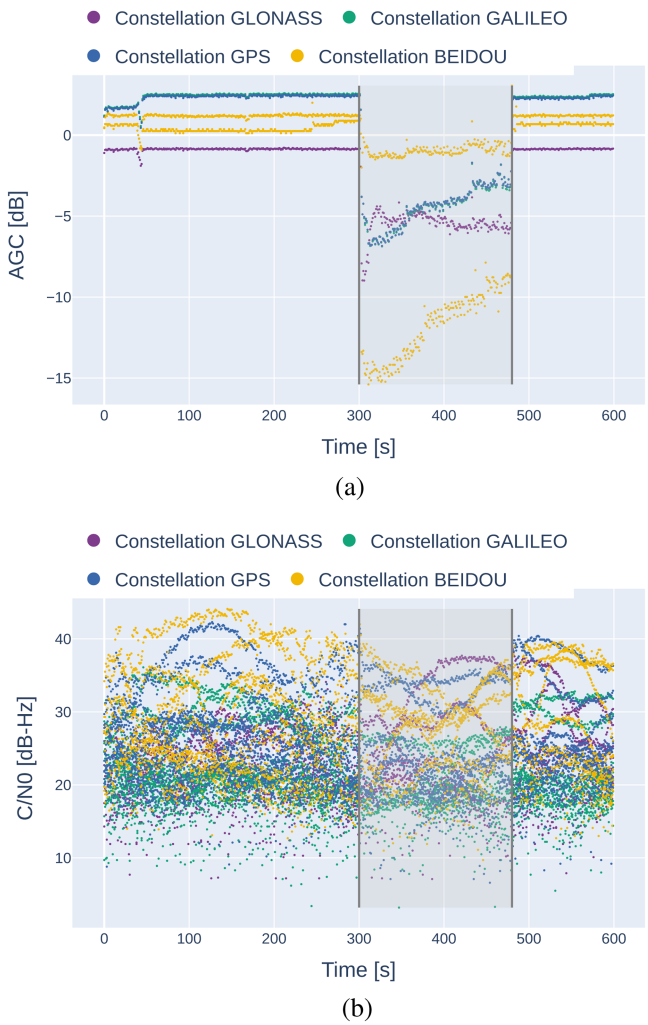

Fig. 8. AGC and C/N_0 time series in the microwave "side" configuration for OnePlus 8 device. The interval corresponding to microwave operation (EMI phase) is indicated by an opaque shaded overlay. (a) AGC trend over time during the experiment. (b) C/N_0 trend over time during the experiment.

total input power and noise, as illustrated in Fig. 1. The digitized signal is then processed by the tracking engine, which separates individual satellite signals and assigns constellation and carrier-frequency identifiers. The receiver firmware records the effective AGC level for each frequency band and reports these values to the Android framework, where they are labeled by both constellation and carrier frequency. Public documentation does not specify how firmware maps band-level AGC readings to constellation-specific entries; however, it is reasonable to hypothesize that implementations may replicate a single band-level value across constellations sharing the same band, or apply small per-constellation adjustments possibly informed by tracking statistics. Consequently, AGC values reported per constellation in Android's GNSS API should be interpreted as "indicative of changes on input signal power in the frequency band" rather than independent per-constellation gain controls [39].

From the heatmaps in Fig. 7, it can be observed that the Oppo Reno exhibits, in all setups, an extremely small ΔAGC [see Fig. 7(a)], with values ranging from 0.24 to 0.50 dB, indicating a poorly responsive gain control or limited dynamic range. This behavior allows the interference to more strongly affect the correlation chain, as confirmed by the $\Delta C/N_0$ values, which reach 2.29 dB-Hz in the front setup and approximately 2 dB-Hz in the side setup. These higher drop values can be explained by the fact that, during the interference, the noise density N_0 increases while the useful signal power remains essentially unchanged, leading to a lower C/N_0 compared to the interference-free case. This aligns with [40], where simultaneous AGC and C/N_0 drops indicate possible jamming. This effect is also reflected in the RMSE metrics: the ΔRMSE_p is consistently high, ranging between 5.1 and 7.06 m. The velocity metric also shows a noticeable impact, with ΔRMSE_v increasing up to 0.175 m/s in the side setup. Moreover, the satellite availability decreases significantly, with a reduction of 15.86% in the front setup and approximately 3.3% in the other two setups, highlighting the impact of interference on signal tracking.

Regarding the OnePlus 8, its behavior differs notably from that observed for the Oppo Reno. This discrepancy is likely due to hardware differences, as reported in the official manufacturer specifications of the devices [41], [42]. The OnePlus 8 exhibits much higher ΔAGC values, ranging from 0.65 up to 6.21 dB, indicating a more responsive AGC that deliberately reduces the gain as interference increases. This allows the interference impact on the correlators to remain limited, as reflected by the relatively moderate $\Delta C/N_0$ values in the front setup (1.12 dB) and in the over setup (0.89 dB). The effectiveness of the OnePlus AGC is particularly evident in the PVT performance, where the ΔRMSE_p remains low in the two above-mentioned setups (0.40 and 0.56 m) and even becomes negative in the side setup. This negative value, which suggests an apparent improvement of the RMSE in the presence of interference, can be interpreted by looking at the corresponding value in Fig. 7(e), where an 18% drop in satellite availability is reported. A plausible explanation is that the satellites lost during tracking may be those at low elevation, which typically exhibit lower C/N_0 values and tend to degrade the position estimation. As for the velocity, the ΔRMSE_v is zero (at least to the third decimal place) in all scenarios.

These findings highlight the varying susceptibility of GNSS receivers to external microwave interference, emphasizing the role of hardware design and supplementary positioning technologies in mitigating signal degradation.

B. Wi-Fi Interference

This section presents the experimental results for the Wi-Fi case. In particular, the results of both urban environment and low-elevation blockage cases are reported in Fig. 9.

From the heatmaps, a behavior similar to the one previously discussed in Section III-A can be observed. In particular, the Oppo Reno shows no adaptation of the AGC value, which results in significant C/N_0 drops: 2.43 dB-Hz in the urban environment and an even stronger 4.1 dB-Hz in the low-elevation blockage scenario. This has a clear impact on the PVT performance, with a ΔRMSE_p drop of 7.44 m in urban environment, and also on

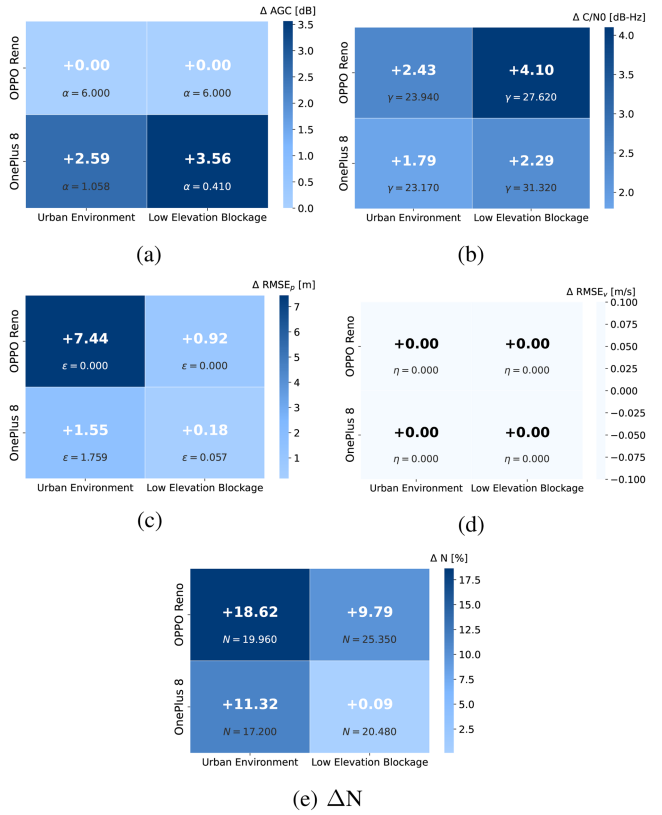

Fig. 9. FoMs for the Wi-Fi experiments (WF-1 and WF-2). (a) ΔAGC. (b) $\Delta C/N_0$. (c) $\Delta RMSE_p$. (d) $\Delta RMSE_v$. (e) ΔN.

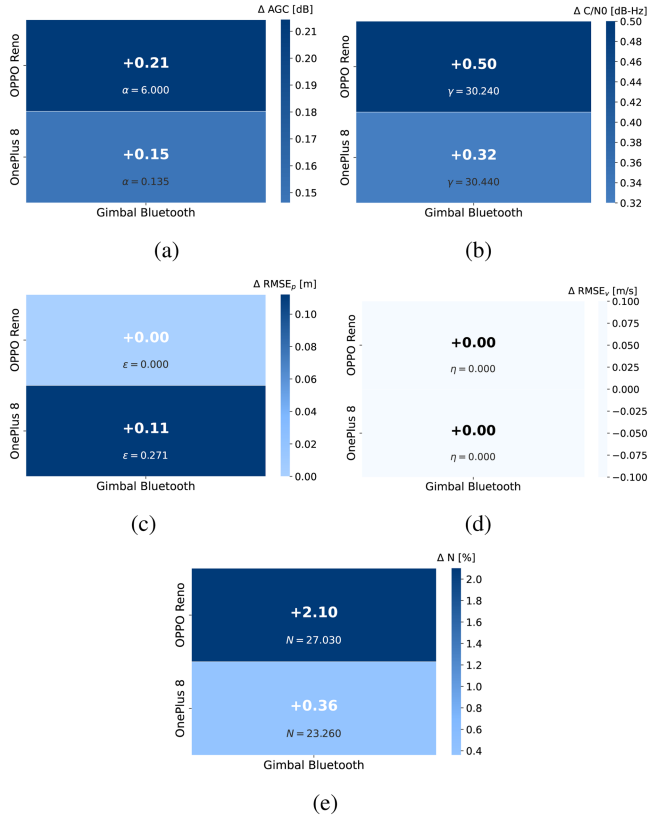

Fig. 10. FoMs for the Bluetooth gimbal experiment (BT-1). (a) ΔAGC. (b) $\Delta C/N_0$. (c) $\Delta RMSE_p$. (d) $\Delta RMSE_v$. (e) ΔN.

satellite availability, which decreases by up to 18.62% in urban environment and 9.79% in the low-elevation blockage scenario.

The OnePlus 8, by contrast, continues to exhibit an active AGC response, with drops of 2.59 and 3.56 dB across the two scenarios. This behavior explains the more limited C/N_0 degradation, respectively, 1.79 dB-Hz in the urban environment and 2.29 dB-Hz in the low-elevation blockage scenario, as seen in Fig. 9(b). Furthermore, because of a large initial C/N_0 level prior to the EMI window ($\gamma = 31.31$ dB-Hz), the C/N_0 drop experienced in the latter scenario results in a negligible impact on the average satellites availability, as shown in Fig. 9(e). Regarding the impact on position accuracy, the degradation remains contained, with values below 2 m in both cases.

As for the velocity solution, for both devices and in both scenarios, the impact is practically negligible.

C. Individual Bluetooth Interference

This section presents the results of the two experiments conducted to evaluate individual Bluetooth interference. The results of the first experiment (BT-1), which includes interference from the gimbal, are presented in Fig. 10. Overall, the results show a negligible impact when compared with the experiments involving microwave and Wi-Fi interference. The drop in satellite availability shown in Fig. 10(e) is minimal and can be attributed to normal satellite losses due to the scenario geometry, this is consistent with the observed minimal drop in C/No. The impact on AGC, as well as on position and velocity, shown, respectively, in Fig. 10(a), (c), and (d), does not exhibit significant variations that can be attributed to the presence of the EMI.

Conversely, the FoMs for the second experiment (BT-2), which involves Bluetooth headphones, are presented in Fig. 11.

Comparing Figs. 7(a) and 11(a), it is evident that the Bluetooth generates a smaller AGC drop than microwave oven, suggesting that Bluetooth has a much weaker impact on the GNSS front-end. Moreover, Fig. 11(b) shows that as the distance of the Bluetooth headphones increases, leading to a corresponding increase in Bluetooth signal power, the C/N_0 drop does not proportionally increase. Instead, in some cases, small gains are even observed. This behavior is characteristic of Bluetooth transmitters, which dynamically adjust their power output as the distance to the receiver increases.

Furthermore, Fig. 11(e) shows that satellite availability remains essentially unaffected across all distances tested, further confirming that Bluetooth interference alone has a minimal impact on GNSS signal integrity and tracking.

In summary, although the second experiment with Bluetooth headphones yielded higher performance degradations compared to the first experiment with the Gimbal, the interference generated by both Bluetooth accessories does not significantly impact GNSS performance across all the evaluated metrics.

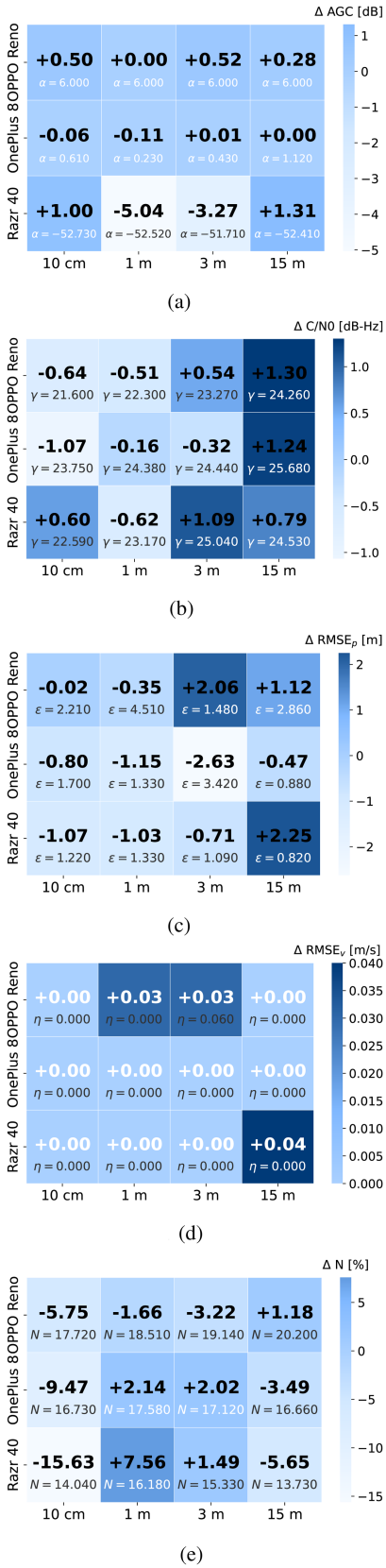

Fig. 11. FoMs for the Bluetooth headphones experiments (BT-2). (a) ΔAGC. (b) ΔC/N_0. (c) Δ$RMSE_p$. (d) Δ$RMSE_v$. (e) ΔN.

D. Crowded Bluetooth Interference

Given the rapid proliferation of Bluetooth-enabled IoT devices, we also investigated a dense interference environment involving Bluetooth emitters.

The results of the crowded Bluetooth interference experiment (BT-3), summarized in Fig. 12 for the *flight-mode* ON, *flight-mode* OFF, and *flight-mode* OFF*and Bluetooth* ONconditions, show that the overall impact of this type of interference on GNSS performance is limited across all devices. AGC drops remain small and inconsistent in sign, indicating that Bluetooth activity in a crowded environment does not trigger a strong or systematic gain-control response.

C/N_0 degradation is similarly limited, with drops mostly within 0.2–1.2 dB, confirming that Bluetooth signals do not significantly affect GNSS signal quality in this environment. Position accuracy is only moderately affected: the OnePlus 40 shows a degradation of 3.11 m in the *Bluetooth*-ONcondition, while the other devices exhibit negative $\Delta RMSE_p$ values, suggesting minor improvements likely caused by the exclusion of low-elevation satellites or small geometry changes rather than direct interference. Velocity performance remains unchanged ($\Delta RMSE_v \approx 0$) for all devices and configurations. Satellite availability is mostly unaffected by Bluetooth interference in this setting.

Overall, these results confirm that Bluetooth interference, whether generated by isolated devices or within a crowded environment, has a minimal effect on GNSS performance in terms of signal strength, PVT accuracy, or satellite tracking.

E. Comparative Analysis

The comparative analysis of GNSS signal degradation across the tested devices, microwave oven, Wi-Fi router, and Bluetooth, reveals distinct interference patterns and levels of impact. Among the three, the microwave oven exhibits the most severe effects, with significant drops in both AGC and C/N_0 values, particularly in the side and front configurations, as shown in Fig. 7(a) and (b). This pronounced degradation, accompanied by a substantial loss in satellite availability, underscores the disruptive nature of these kind of microwave-induced EMI, aligning with previous findings.

In contrast, the Wi-Fi router shows a more mitigated impact. While the low-elevation blockage scenario results in greater signal degradation than the urban environment (see Fig. 9), the corresponding satellites availability loss remains comparatively low with respect to the latter. This suggests that although Wi-Fi interference affects signal quality, it does not critically impair the GNSS-based PVT estimation capability.

Instead, for what concerns Bluetooth interference, it exhibited the least impact on GNSS performance. The experiments demonstrate minimal AGC and C/N_0 drops, with no clear correlation between signal power and degradation, as shown in Figs. 10(a) and 10(b), 11(a) and 11(b), and 12(a) and 12(b).

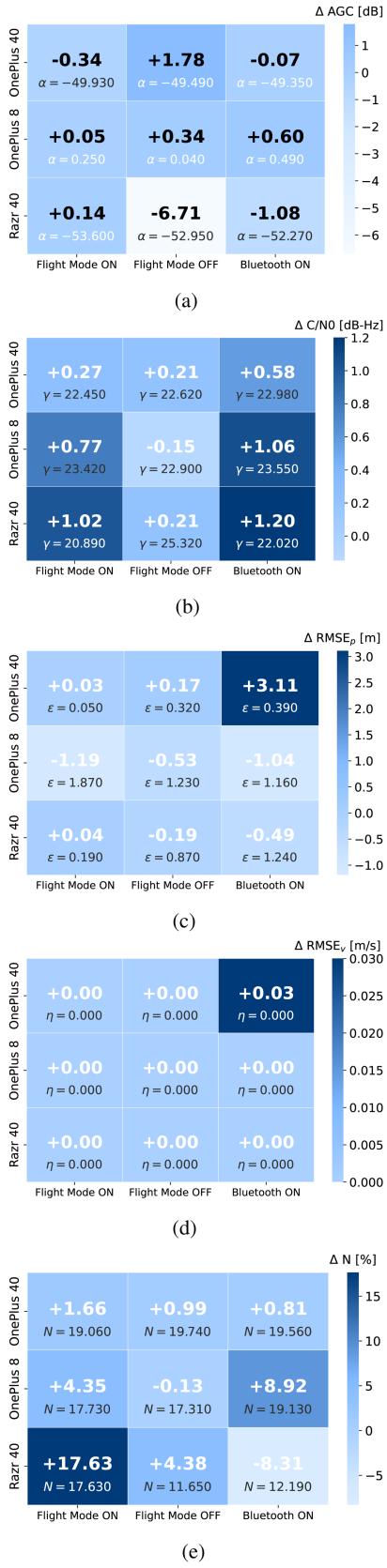

Fig. 12. FoMs for the crowded Bluetooth environment experiments (BT-3). (a) ΔAGC. (b) ΔC/N_0. (c) Δ$RMSE_p$. (d) Δ$RMSE_v$. (e) ΔN.

Device-specific analyses also reveal interesting disparities. The OPPO phone generally experiences lower AGC drops but higher C/N_0 reductions compared to the OnePlus 8. These differences likely stem from variations in hardware design and the use of auxiliary positioning technologies, such as A-GPS and WLAN-based positioning, which can mitigate GNSS signal degradation [1].

Overall, the microwave oven poses the highest interference threat to GNSS performance, followed by Wi-Fi, with Bluetooth showing negligible effects under the tested conditions.

IV. Conclusion

This study investigated the impact of unintentional EMI from common household and consumer electronic devices on GNSS performance in Android smartphones. A series of controlled experiments evaluated the effects of microwave ovens, Wi-Fi routers, and Bluetooth emitters, including both isolated devices and crowded scenarios, on AGC behavior, C/N_0 levels, positioning accuracy, velocity estimation, and satellite availability.

The results demonstrate that the microwave oven generates the most significant interference, causing the largest degradations across all performance metrics. Wi-Fi interference produces moderate effects, whereas Bluetooth, both in single-device and dense environments, has a minimal impact under the tested conditions.

While household appliances and consumer electronics may not pose a significant threat to GNSS receivers in urban environments, and despite the distinct impacts of each analyzed device on GNSS performance, the overall implication is that GNSS receivers are inherently vulnerable to various forms of localized EMI and require appropriate protective measures—especially as the density of potential EMI sources is expected to increase in future urban environments. Nevertheless, it is worth noting that, due to the use of COTS devices and the lack of access to detailed RF characteristics, this study focuses on the observable impact of EMI rather than on isolating its specific physical origin, which would require controlled signal generation and device-level analysis.

Finally, variations in interference susceptibility across different smartphone models highlight the need for standardized testing frameworks that account for diverse chipset architectures and auxiliary positioning methods. Future research should investigate the cumulative and synergistic effects of multiple coexisting EMI sources, along with potential mitigation strategies designed to address the evolving landscape of consumer electronics. Moreover, extending the experimental campaign to a broader and more diverse range of device models and brands could help strengthen the generalizability of the conclusions, and is suggested as an avenue for future work. By integrating these insights into both receiver design and regulatory guidelines, the resilience and accuracy of GNSS-based applications can be more effectively safeguarded in rapidly changing electromagnetic environments.

REFERENCES

[1] F. Van Diggelen, *A-GPS: Assisted GPS, GNSS, and SBAS*. Norwood, MA, USA: Artech House, 2009.

[2] A. Minetto, A. Nardin, and F. Dovis, "Modelling and experimental assessment of inter-personal distancing based on shared GNSS observables," *Sensors*, vol. 21, no. 8, 2021, Art. no. 2588. [Online]. Available: https://www.mdpi.com/1424-8220/21/8/2588

[3] A. Minetto, M. C. Bello, and F. Dovis, "Corrections to "DGNSS cooperative positioning in mobile smart devices: A proof of concept"," *IEEE Trans. Veh. Technol.*, vol. 74, no. 10, pp. 16648–16661, Oct. 2025.

[4] A. Nardin, "Innovative signal processing solutions for next-generation satellite navigation systems," Ph.D. dissertation, Politecnico di Torino, Torino, Italy, 2023. [Online]. Available: https://hdl.handle.net/11583/2979890

[5] A. Joseph and M. Petovello, "Measuring GNSS signal strength," *Inside GNSS*, vol. 5, no. 8, pp. 20–25, 2010.

[6] F. Dovis, *GNSS Interference, Threats, and Countermeasures*. Norwood, MA, USA: Artech House, 2015.

[7] M. L. Psiaki and T. E. Humphreys, "GNSS spoofing and detection," *Proc. IEEE*, vol. 104, no. 6, pp. 1258–1270, Jun. 2016.

[8] G. X. Gao, M. Sgammini, M. Lu, and N. Kubo, "Protecting GNSS receivers from jamming and interference," *Proc. IEEE*, vol. 104, no. 6, pp. 1327–1338, Jun. 2016.

[9] N. Spens, D.-K. Lee, F. Nedelkov, and D. Akos, "Detecting GNSS jamming and spoofing on android devices," *NAVIGATION: J. Inst. Navigation*, vol. 69, no. 3, pp. 1–15, 2022. [Online]. Available: https://navi.ion.org/content/69/3/navi.537

[10] A. Nardin, T. Imbiriba, and P. Closas, "Jamming source localization using augmented physics-based model," in *Proc. ICASSP 2023-2023 IEEE Int. Conf. Acoust., Speech Signal Process.*, 2023, pp. 1–5.

[11] A. Nardin, T. Imbiriba, and P. Closas, "Crowdsourced jammer localization using APBMs: Performance analysis considering observations disruption," in *Proc. IEEE/ION Position, Location Navigation Symp.*, 2023, pp. 511–519.

[12] M. Jaramillo Civill, P. Wu, A. Nardin, T. Imbiriba, and P. Closas, "Jammer source localization with federated learning," in *Proc. IEEE/ION Position, Location Navigation Symp.*, 2025, pp. 362–371.

[13] S. Thombre et al., "GNSS threat monitoring and reporting: Past, present, and a proposed future," *J. Navigation*, vol. 71, no. 3, pp. 513–529, 2018.

[14] S. Jada, J. Bowman, M. Psiaki, S. Langel, and M. Joerger, "Identifying car key fobs as a cause of interference at GNSS frequencies," in *Proc. 36th Int. Tech. Meeting Satell. Division Inst. Navigation*, 2023, pp. 4110–4120, doi: 10.33012/2024.19646.

[15] G. Tsintsadze, H. Manoharan, A. Sahai, D. Beetner, and B. Booth, "Evaluating electromagnetic interference effects on GNSS receivers," in *Proc. IEEE Int. Symp. Electromagn. Compat., Signal & Power Integrity*, 2024, pp. 308–312.

[16] J. F. M. Lorga et al., "GNSS hybridization for indoor positioning," in *Proc. 5th ESA Workshop Satell. Navigation Technol. Eur. Workshop GNSS Signals Signal Process.*, 2010, pp. 1–13.

[17] Z. Li, N. Zhu, and V. Renaudin, "Self-contained pedestrian navigation fusing ML-selected GNSS carrier phase and inertial signals in challenging environments," *IEEE J. Indoor Seamless Positioning Navigation*, vol. 2, pp. 177–192, 2024.

[18] T. Lin, M. Ma, A. Broumandan, and G. Lachapelle, "Demonstration of a high sensitivity GNSS software receiver for indoor positioning," *Adv. Space Res.*, vol. 51, no. 6, pp. 1035–1045, 2013. [Online]. Available: https://www.sciencedirect.com/science/article/pii/S0273117712003845

[19] Y. Wang et al., "GPMS: Enabling indoor GNSS positioning using passive metasurfaces," in *Proc. 30th Annu. Int. Conf. Mobile Comput. Netw.*, ser. ACM MobiCom '24, New York, NY, USA, 2024, pp. 1424–1438, doi: 10.1145/3636534.3690702.

[20] A. Dhaliwal, "The rise of automation and robotics in warehouse management," in *Transforming Management Using Artificial Intelligence Techniques*. Boca Raton, FL, USA: CRC Press, 2020, pp. 68–70.

[21] M. Vollmer, "Physics of the microwave oven," *Phys. Educ.*, vol. 39, no. 1, 2004, Art. no. 74.

[22] E. Kaplan and C. Hegarty, *Understanding GPS/GNSS: Principles and Applications*. Norwood, MA, USA: Artech House, 2017.

[23] J. Florwick, J. Whiteaker, A. C. Amrod, and J. Woodhams, "Wireless LAN design guide for high density client environments in higher education," Cisco Systems, San Jose, CA, USA, Tech. Rep., 2017.

[24] L. Zhu, C. Lin, K. Meng, and X. Tang, "An experimental analysis of interference in 802.11n wireless mesh networks," in *Proc. 2013 15th IEEE Int. Conf. Commun. Technol.*, 2013, pp. 276–280.

[25] D. Dardari, P. Closas, and P. M. Djurić, "Indoor tracking: Theory, methods, and technologies," *IEEE Trans. Veh. Technol.*, vol. 64, no. 4, pp. 1263–1278, Apr. 2015.

[26] M. Ramella, "Receiver architectures for SoC coexistence," Ph.D. dissertation, Università degli Studi di Pavia, Pavia, Italy, 2015 . [Online]. Available: http://www-9.unipv.it/dottMICR/theses/Ramella.pdf

[27] P. Dabove and V. Di Pietra, "Towards high accuracy GNSS real-time positioning with smartphones," *Adv. Space Res.*, vol. 63, no. 1, pp. 94–102, 2019. [Online]. Available: https://www.sciencedirect.com/science/article/pii/S0273117718306537

[28] F. Zangenehnejad and Y. Gao, "GNSS smartphones positioning: Advances, challenges, opportunities, and future perspectives," *Satell. Navigation*, vol. 2, no. 1, Nov. 2021, Art. no. 24, doi: 10.1186/s43020-021-00054-y.

[29] I. Ebrahimi Mehr, "Modern approaches for GNSS interference monitoring and analysis," Ph.D. thesis, Politecnico di Torino, Torino, Italy, 2025. [Online]. Available: https://hdl.handle.net/11583/3004953

[30] European GNSS Agency (GSA), "Using GNSS raw measurements on android devices: Towards better location performance in mass market applications," European GNSS Agency (GSA), White Paper, Jan. 2018. [Online]. Available: https://www.euspa.europa.eu/publications-multimedia/publications/using-gnss-raw-measurements-android-devices

[31] M. Russo, C. Carallo, R. Tommasi, and A. Nardin, "Electromagnetic interference from consumer electronics on GNSS performance in smartphones," in *Proc. Int. Conf. Localization GNSS*, 2025, pp. 1–7.

[32] European Parliament and the Council of the European Union, "Directive 2014/30/EU of 26 February 2014 on the harmonisation of the laws of the Member States relating to electromagnetic compatibility (recast)," *Official J. Eur. Union*, L96, pp. 79–106, Mar. 29, 2014, [Online]. Available: http://data.europa.eu/eli/dir/2014/30/2018-09-11

[33] F. Dovis, *GNSS Interference Threats and Countermeasures, Ser. The GNSS Technology and Application Series*. Norwood, MA, USA: Artech House, 2015.

[34] Google, "GPS measurement tools," 2024. [Online]. Available: https://github.com/google/gps-measurement-tools

[35] D.-K. Lee, N. Spens, B. Gattis, and D. Akos, "AGC on Android devices for GNSS," in *Proc. 2021 Int. Tech. Meeting (ITM) Inst. Navigation*, 2021, pp. 33–41.

[36] F. Darugna, J. Wübbena, A. Ito, T. Wübbena, G. Wübbena, and M. Schmitz, "RTK and PPP-RTK using smartphones: From short-baseline to long-baseline applications," in *Proc. 32nd Int. Tech. Meeting Satell. Division Inst. Navigation*, Miami, FL, USA, Sep. 2019, pp. 3932–3945.

[37] J. Yun, C. Lim, and B. Park, "Inherent limitations of smartphone GNSS positioning and effective methods to increase the accuracy utilizing dual-frequency measurements," *Sensors*, vol. 22, no. 24, 2022, Art. no. 9879. [Online]. Available: https://www.mdpi.com/1424-8220/22/24/9879

[38] I. Mozharovskyi, "Ping - network utility," 2025. [Online]. Available: https://apps.apple.com/it/app/ping-network-utility/id576773404

[39] The Android Open Source Project (2022), "GnssAutomaticGainControl API reference," Accessed 3 Nov. 2025. [Online]. Available: https://developer.android.com/reference/android/location/GnssAutomaticGainControl

[40] E. G. Manfredini, D. M. Akos, Y.-H. Chen, S. Lo, T. Walter, and P. Enge, "Effective GPS spoofing detection utilizing metrics from commercial receivers," in *Proc. Int. Tech. Meeting Inst. Navigation*, Reston, VA, USA, Jan. 2018, pp. 672–689, doi: 10.33012/2018.15595.

[41] OnePlus, "Oneplus 8 specifications," 2025, Accessed: Feb. 22, 2025. [Online]. Available: https://www.oneplus.com/it/8/specs

[42] OPPO, "Oppo Reno11 F specifications," 2025, Accessed: Feb. 22, 2025. [Online]. Available: https://www.oppo.com/en/smartphones/series-reno/reno11-f/specs/